catalysts

MDPI

Article

Facet-Dependent Interfacial Charge Transfer in TiO_2/Nitrogen-Doped Graphene Quantum Dots Heterojunctions for Visible-Light Driven Photocatalysis

Nan-Quan Ou [1,†], Hui-Jun Li [1,†], Bo-Wen Lyu [1], Bo-Jie Gui [1], Xiong Sun [1], Dong-Jin Qian [2], Yanlin Jia [3,4,*], Xianying Wang [1,5,*] and Junhe Yang [1,5]

1 School of Materials Science and Technology, University of Shanghai for Science and Technology, Shanghai 200093, China; ounanquan@163.com (N.-Q.O.); huijunli0701@126.com (H.-J.L.); bowenlyu0324@163.com (B.-W.L.); bojie_gui@163.com (B.-J.G.); sunxiong1993@163.com (X.S.); jhyang@usst.edu.cn (J.Y.)
2 Shanghai Key Laboratory of Molecular Catalysis and Innovative Materials, Fudan University, Shanghai 200433, China; djqian@fudan.edu.cn
3 College of Materials Science and Engineering, Central South University, Changsha 410083, China
4 College of Materials Science and Engineering, Beijing University of Technology, Beijing 100124, China
5 Shanghai Innovation Institute for Materials, Shanghai 200444, China
* Correspondence: xianyingwang@usst.edu.cn (X.W.); jiayanlin@126.com (Y.J.)
† These two authors contributed equally to this work.

Received: 26 February 2019; Accepted: 8 April 2019; Published: 9 April 2019

Abstract: Interfacial charge transfer is crucial in the efficient conversion of solar energy into fuels and electricity. In this paper, heterojunction composites were fabricated, comprised of anatase TiO_2 with different percentages of exposed {101} and {001} facets and nitrogen-doped quantum dots (NGQDs) to enhance the transfer efficiency of photo-excited charge carriers. The photocatalytic performances of all samples were evaluated for RhB degradation under visible light irradiation, and the hybrid containing TiO_2 with 56% {001} facets demonstrated the best photocatalytic activity. The excellent photoactivity of TiO_2/NGQDs was owed to the synergistic effects of the following factors: (i) The unique chemical features of NGQDs endowed NGQDs with high electronic conductivities and provided its direct contact with the TiO_2 surface via forming Ti–O–C chemical bonds. (ii) The co-exposed {101} and {001} facets were beneficial for the separation and transfer of charge carriers in anatase TiO_2. (iii) The donor-acceptor interaction between NGQDs and electron-rich {101} facets of TiO_2 could remarkably enhance the photocurrent, thus hindering the charge carriers recombination rate. Extensive characterization of their physiochemical properties further showed the synergistic effect of facet-manipulated electron-hole separation in TiO_2 and donor-acceptor interaction in graphene quantum dots (GQDs)/TiO_2 on photocatalytic activity.

Keywords: electron transfer; graphene quantum dots; heterojunction; photocatalysis; TiO_2

1. Introduction

Anatase TiO_2 is generally considered a better photocatalyst than rutile, mainly due to its attributes of longer exciton diffusion length, higher electron mobility, and longer carrier life time [1,2]. The photocatalytic activity of anatase has been revealed to depend closely on the crystal surface [3,4]. Clear pictures have now shown that reduction and oxidation reactions would preferentially occur on {101} and {001} facets, respectively. Furthermore, it has been found that the {101} surface is attractive for electrons in aqueous solutions while excess electrons tend to strongly avoid the {001} surface via surface

science experiments and first-principles simulations [5]. The substantial electrons in anatase TiO_2 generated via photoexcitation play an important part in many energy-related applications. However, due to intrinsic defects and the fast carrier recombination rate, electron trapping in anatase TiO_2 are unavoidable, which hamper the overall photocatalytic activity [6,7].

To solve this problem, fabrication of heterojunctions modified anatase TiO_2 has emerged as a promising method [8–10]. Angus and co-workers reported the development of a hetero-structured material by using pre-formed carbon nitride nanosheets (CNNS) composite with facet-controllable TiO_2. The materials possess an excellent CO_2 adsorption capacity and charge transfer rate, thus leading to the improvement of the photocatalytic activity of TiO_2 [11]. Luca Rimoldi et al. have then reported a method to combine TiO_2 with WO_3. Due to the admirable properties of WO_3, the photocatalytic activity enhanced remarkably [12]. Through a series of experiments and calculations, Latterly Olowoyo et al. have also found that carbon nanotubes (CNTs) can strongly be attached to the {101} facet of TiO_2, since the atomic orbitals of anatase overlap with the orbitals of the CNTs [13].

As a novel class of quantum dots (QDs), graphene quantum dots (GQDs) have currently attracted intensive interest in fabricating new heterojunctions, due to their large surface areas, high electron mobilities, conductivity, and adjustable band gaps [14,15]. These properties ensure discrete electronic levels, which could allow for light-induced electron injection, efficient carrier transfer, and long-lived excited states [16–20]. GQDs have also been explored as the light absorber and heteroatoms-doped GQDs are expected to realize absorption in the visible region [21]. A variety of surface functional groups on GQDs could provide better covalent chemical linking between anatase and GQDs, facilitating charge separation and transfer behaviors [22–24]. Pan et al. have found that monodispersed amine-functionalized GQDs anatase TiO_2 heterojunctions have an absorption range extended into the visible light region and a much lower carrier recombination rate. They attributed the improved performance to the proper energy position of GQDs/TiO_2 23]. Then, Yu and co-workers reported the decoration of GQDs on {001} faceted anatase TiO_2 with an exposed percentage of 65%–75%. The experiments show a promotion of photocatalytic hydrogen evolution rate of the composites compared to bare anatase, which might originate from the higher-charge separation efficiency. [25] Zheng and co-workers also utilized TiO_2 and sulfur, nitrogen co-doped GQDs (SN-GQDs) to develop an efficient photocatalyst for synthesizing H_2O_2. They testified that SN-GQDs induced visible light absorption, promoted charge transfer, and provided active sites for ·OOH formation [26]. Recently, Prezhdo et al. built several models of donor-acceptor interaction between GQDs and TiO_2 via stacking and covalent bonding, respectively, to provide guidance for subsequent photocatalysis application [16].

These findings provide strong evidence and also motivation for deeply understanding the models of electron-hole separation dynamics at heterojunction interfaces [3,21,27,28]. There has still been no adequate investigation, considering the influence of facet-dependent photogenerated charge-carrier separation in anatase TiO_2, on the photocatalytic activity of GQDs/TiO_2. Since both theoretical and experimental studies had shown that {101} crystal facets are electron-rich while {001} crystal facets are hole-rich in anatase TiO_2, it would be desirable to elucidate the different donor-acceptor interaction between NGQDs and TiO_2 with specific facet composition, thus providing explicit guidance in constructing heterojunction structures with superior performance.

Herein, we have designed a heterojunction composite via depositing nitrogen-doped GQDs on anatase TiO_2 with different exposure percentages of {001} and {101} facets, combining the advantages of facet and interfacial modification to maximize the driving force promoting charge carrier transfer. The visible light-driven dye degradation performances on anatase TiO_2 with {101}, {001}, and {001}-{101} facets, and their corresponding heterojunctions with nitrogen-doped GQDs (NGQDs) have been systematically studied. To further understand the electron transfer mechanism, the relationships of the morphology, chemical states, optical, and electrical properties with the photocatalytic activity were intensively analyzed.

2. Results and Discussion

2.1. Structural Characterization

The crystalline phases of different samples before and after decoration with NGQDs were firstly identified. Figure 1 shows the X-ray diffraction (XRD) patterns of anatase TiO_2 with different exposed facets. The diffraction peaks appeared around 2θ values of 25.3, 38.6, 48.0, 53.9, and 62.1, assigned to the (101), (112), (200), (105), and (213) crystal planes of anatase titania, respectively [27]. For bare anatase TiO_2, with the increase of Hydrofluoric acid (HF) volume, the {004} diffraction peak was broadened, implying the thickness of the TiO_2 along the {001} direction was decreased. Meanwhile, the intensity of the {200} diffraction peaks was enhanced, indicative of the increasing side length of the nanoparticles along the {100} direction. According to the two peaks, the percentage of the exposed {001} facet could be estimated, based on the calculation method reported in the literature. Shown in Table 1, the percentage was increased when increasing the HF volume [29]. The calculation method was described in the supporting information, as shown in Figure S1. By comparison, the XRD patterns of TiO_2/NGQDs exhibited similar but much lower diffraction peaks. The XRD pattern of NGQDs showed a wide weak diffraction peak centered at 26.8°, assigned to the {002} facet [30]. Though the diffraction peak of NGQDs was not observed in the composites, which might be due to the relatively low diffraction intensity of NGQDs, the peak attributed to the {101} facet of anatase decreased obviously. The possible reason is that the {002} crystal orientation in NGQDs influenced the {101} surface of TiO_2, thus leading to decrease of the peak [31].

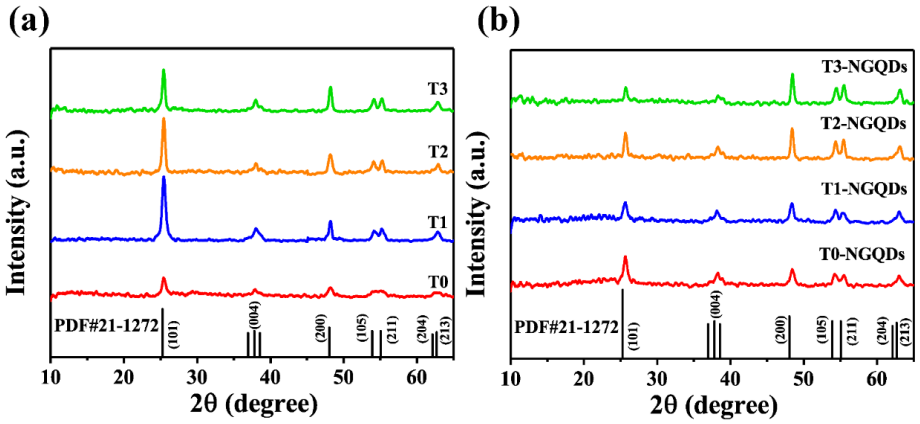

Figure 1. XRD patterns of different samples (**a**) without and (**b**) with nitrogen-doped quantum dots (NGQDs) decoration.

Table 1. Structural information of different anatase titania samples.

Samples	Average thickness (nm)	Average length (nm)	Percentage of {001}
T0	8.9	8.1	12%
T1	8.5	13.8	56%
T2	6.1	21.6	71%
T3	4.3	25.5	85%

In Raman spectroscopy, all samples show similar peaks centered at 144, 394, 514, and 636 cm^{-1} shown in Figure S2. When increasing the addition amount of HF, the intensity of the Eg peak at 144 cm^{-1} decreased simultaneously. The Eg peak is mainly attributed to the symmetric stretching vibration of O−Ti−O TiO_2 [29]. A higher percentage of exposed {001} facets generally represented fewer amount of symmetric O−Ti−O stretching vibration modes, thus leading to the decreasing intensity of Eg peak in the Raman spectra. Thus, it could be concluded from the Raman spectra that the exposure percentage of {001} facets increased with the increase of HF volume. Shown in the inset of Figure

S2b, two characteristic peaks of D and G band appeared at 1351 cm^{-1} and 1590 cm^{-1}, respectively, confirming the presence of graphite-like structure in the composites.

X-ray photoelectron spectroscopy (XPS) spectra were measured to study the bonding conditions in the heterojunctions, shown in Figure 2. The Ti 2p spectra showed two peaks with the binding energies of 458.9 eV and 464.6 eV, which are assigned to Ti $2p^{3/2}$ and $2p^{1/2}$ spin-orbital splitting photoelectrons, respectively. The splitting values indicated Ti^{4+} chemical states in these samples, while no Ti^{3+} forms were observed [32]. The C 1s spectra could be then fitted into three Gaussian peaks (288.8 eV, 286.1 eV, and 284.8 eV). The peak at 288.8 eV was assigned to the sp^2 hybridized carbon in the skeleton of NGQDs and also some carbon contaminants from the ambience. The other two peaks corresponded to the oxygenated carbon, representative of carboxyl carbon (288.8 eV) and hydroxyl carbon (286.1 eV) functional groups, respectively [33–36]. No Ti–C bond related peak (282 eV) was observed, implying that the NGQDs were probably anchored to the surface of TiO_2 via Ti–O–C bonds. In some reported studies, functional groups including C–O and COOH were evaluated to identify the existence of Ti–O–C bonding [32,37]. These groups are not that stable and might be converted to the epoxy group during the composite formation process.

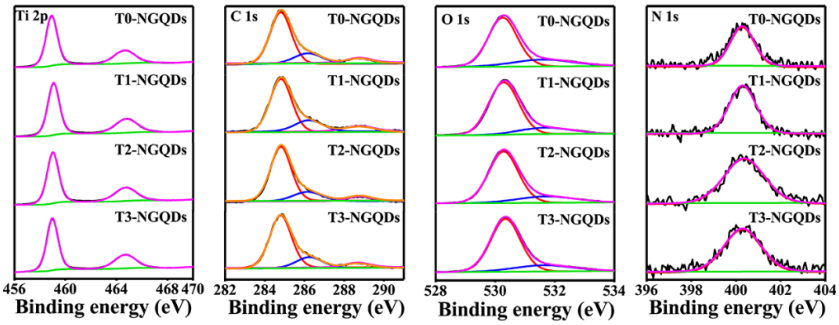

Figure 2. XPS spectra of different TiO_2/NGQDs composites.

The evidence of Ti–O–C bonding formation was further provided in the O 1s XPS spectra. It was fitted into two symmetric peaks. The peaks at 530.3 eV is ascribed to the oxygen in crystal lattice (Ti–O–Ti) and the other peak at 531.6 eV is believed to result from the Ti–O–C bonding, based on previously reported cases [25,32,38]. These results indicated the composite formation of TiO_2/NGQDs through the C–O–Ti bonds. The C–O–Ti bonds are capable of mediating the coupling between NGQDs and TiO_2, which could promote the interfacial electron transfer. The N 1s spectra revealed a peak centered at 400.3 eV, which could be assigned to the pyrrolic N (400.5 eV). The nitrogen atoms are mainly introduced by the NGQDs, demonstrating the successful decoration of NGQDs on the surface of TiO_2 [30]. Furthermore, the percentages of different bonds according to the fitting results of the XPS high-resolution spectra were calculated, shown in Table 2 and Table S1. Similar percentages implied similar bonding and chemical composition in different composites.

Table 2. Percentages of different bonds according to the fitting results of the XPS high-resolution spectra calculated from Figure 2.

Bond	T0-NGQDs	T1-NGQDs	T2-NGQDs	T3-NGQDs
% of Ti 2p	26.57	27.63	27.23	27.69
% of C 1s	21.18	19.4	20.65	18.99
O–C=O/Ti–O–C 288.8 eV	7.91	8.03	7.84	7.83
C–O 286.1 eV	19.53	20.30	19.05	19.26
C=C 284.8 eV	72.56	71.07	73.40	73.34
% of O 1s	51.69	52.33	51.53	52.85
Ti–O–Ti 530.3 eV	77.80	80.97	80.84	80.42
Ti–O–C 531.6 eV	22.20	19.03	19.16	19.58
% of N 1s	0.55	0.64	0.58	0.47

2.2. Morphology Characterization

The morphology of anatase TiO_2 with and without NGQDs decoration were characterized by Transmission Electron Microscope (TEM) and High Resolution Transmission Electron Microscope (HR-TEM). The morphology and crystal facets of TiO_2 remained similar before and after NGQDs modification, as can be seen from Figure 3 and Figure S3. Figure S3 shows that sample T0 is mostly composed of nanoparticles with a truncated octahedral bipyramid. After adding HF into the reaction system, it could be found that the anatase TiO_2 mostly consists of nanoplates and the plate size increases with the increase of HF volume, which is consistent with the XRD calculation results. Figure S4 shows the TEM image of NGQDs, which has an average size of ~2.4 nm. Clear lattice fringes demonstrative of its well-crystalline structure, and the autocorrelated HRTEM lattice image (inset in Figure S4b) show a 0.21 nm lattice fringe assigned to the {100} plane of GQDs [39,40].

The formation of NGQDs/TiO_2 heterojunctions could be obviously observed in the TEM images, shown in Figure 3, of which the NGQDs were uniformly decorated on both {001} and {101} facets of TiO_2. The NGQDs are shown with red circles. No selective deposition of NGQDs on a specific facet of anatase TiO_2 was found. The autocorrelated HRTEM lattice image (inset in Figure 3c,f) both show 0.21 nm lattice fringes assigned to the {100} plane of GQDs. Meanwhile, the autocorrelated HRTEM lattice image (inset in Figure 3c,f) also show clear lattice fringes of 0.35 nm and 0.19 nm, which could be assigned to the {101} and {001} facet of TiO_2, respectively. The HRTEM lattice images of all composites show that the lattices of both NGQDs and TiO_2 are simultaneously recognized, revealing good attachment of NGQDs over the TiO_2 surface.

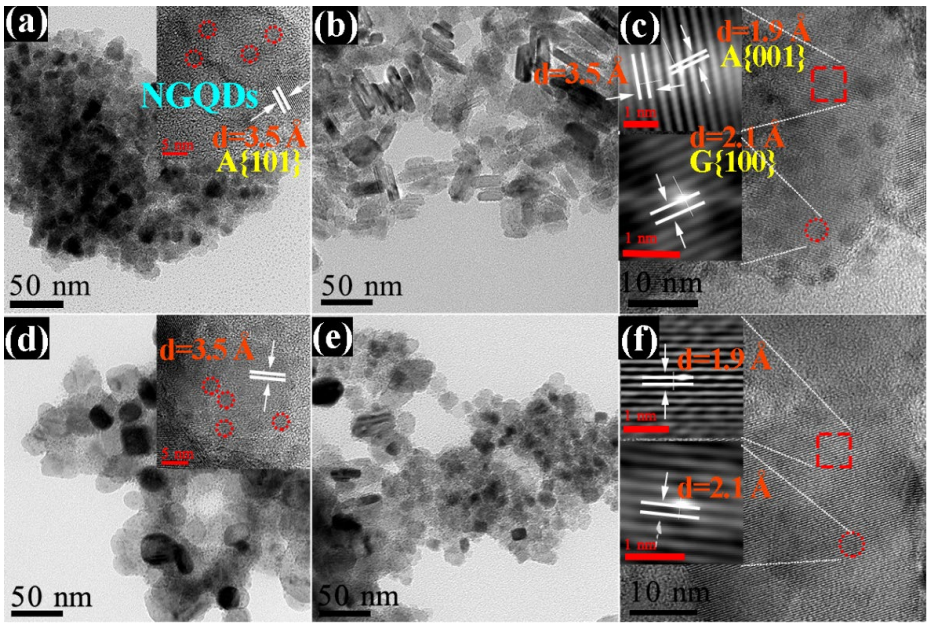

Figure 3. TEM images of (**a**) T0-NGQDs, (**b**,**c**) T1-NGQDs, (**d**) T2-NGQDs, and (**e**–**f**) T3-NGQDs. The inset in (**a**) is the HR-TEM image of T0-NGQDs. The inset in (**c**) is the autocorrelated HRTEM lattice images recorded from the corresponding selected areas. The inset in (**d**) is the HRTEM image of T2-NGQDs. The inset in (**f**) is the autocorrelated HRTEM lattice images recorded from the corresponding selected areas.

2.3. Optical and Electrical Properties

The optical properties of all samples were investigated via the Ultraviolet-Visible (UV-Vis) diffuse reflection spectroscopy (UV-DRS). All anatase TiO_2 demonstrate an absorption threshold near 400 nm in the ultraviolet region. The band gaps of the anatase could be obtained based on the Kubelka–Munk rule, seen from the inset in Figure 4a. The band gaps of T0, T1, T2, and T3 are 3.22, 3.28, 3.30, and 3.32 eV, respectively. Apparently, with the increase of the {001} facet percentage, the light absorption

edge was slightly blue shifted [21]. The UV-vis spectrum of NGQDs is shown in Figure S4d, and the band gap was approximately 1.56 eV, according to our previous work [30,41]. After decorating NGQDs, it was found that there was an increasing visible light absorption for all composites. Generally, the resultant extended light absorption was due to the existence of Ti–O–C chemical bonds between GQDs and TiO_2 [32,37]. The interaction could improve the interfacial carrier transfer rate, which is beneficial to photocatalysis under visible light irradiation. Meanwhile, the presence of the energy gap of NGQDs further ensured the long-lived excited states and absorbance of solar photons in the broad solar spectrum.

The electrochemical Mott–Schottky experiments of the anatase were then measured (Figure 4c). The plots present a positive slope and the flat band potential values were recalculated vs. NHE (Normal Hydrogen Electrode). Combined with the band gaps of anatase TiO_2 and NGQDs, we proposed electronic band structures for all composites, shown in Figure 4d. It was hypothesized that the downshift of conduction band (CB) band level of the anatase might make the electrons less reductive and also weaken the dynamics of the electron transfer rate between TiO_2 and NGQDs [42–44].

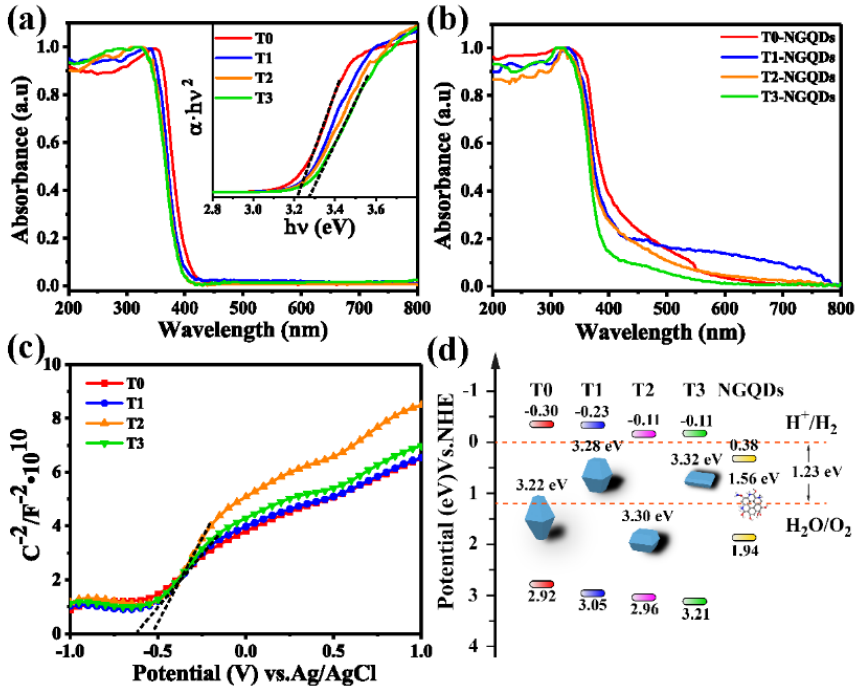

Figure 4. UV-vis diffuse reflection spectra (UV-DRS) of (**a**) bare anatase TiO_2, (**b**) TiO_2/NGQDs composites, (**c**) Mott–Schottky plots of bare anatase TiO_2, and (**d**) band structure diagram of different samples and NGQDs. The inset in (**a**) is the Tauc plot of the corresponding bare anatase TiO_2.

Moreover, the photogenerated charge carrier separation and transfer rate was determined using photocurrent responses, shown in Figure 5. Fast and uniform photocurrents with good reproducibility was demonstrated, indicative of relatively reversible photo-responses. Via three on-off cycles under visible light irradiation (>420 nm), it was found that the photocurrent density of bare anatase TiO_2 decreased in the order of T2, T3, T1, and T0. This suggests that defects (oxygen vacancies) are possibly formed on the surface of pristine anatase TiO_2 with small size under light illumination in our work, which would introduce defect energy levels in the band gap and lead to electron-hole separation under visible light irradiation [25]. Meanwhile, the synergistic effect of {001} and {101} facets would also affect the charge carrier separation efficiency, resulting in the difference of photocurrent.

After depositing NGQDs, their corresponding photocurrent responses were all enhanced obviously. The photocurrent density of TiO_2/NGQDs composites decreased in the order of T1-NGQDs, T2-NGQDs, T0-NGQDs, and T3-NGQDs. The photocurrent density of sample T1-NGQDs was the highest, about

three times larger than that of sample T3-NGQDs. The photocurrent enhancement could be attributed to the promoted separation rate of photogenerated charge carriers, owing to the introduction of NGQDs. The unique chemical features of NGQD endow it with superior carrier mobility and excellent electronic conductivity [45,46]. Moreover, the extended π-electron systems of NGQD provide its sufficient contact with the surface of titania, and the formation of Ti–O–C bonding could also facilitate the donor-acceptor interaction [16]. These factors contributed to the apparent enhancement of photocurrent density. We calculated multiple times the photocurrents of the anatase TiO_2 with and without NGQDs decoration, shown in Figure 5c. Interestingly, the times decreased with the decrease of exposed {101} facet percentage in TiO_2. The phenomenon indicated a noticeable improvement of electron-hole separation efficiency between the NGQDs and the electron-rich {101} facet, compared to that between the NGQDs and the hole-rich {001} facet. The difference demonstrated that efficient electron transfer existed in the interfacial interaction between NGQDs and TiO_2 with high {101} facet exposure.

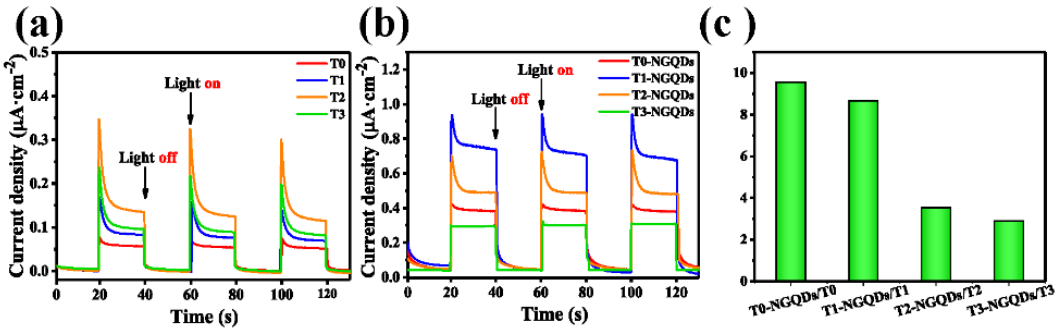

Figure 5. Periodic on-off photocurrent output of (**a**) bare anatase TiO_2, and (**b**) TiO_2/NGQDs composites. (**c**) The multiple times of the photocurrents of the anatase TiO_2 with and without NGQDs decoration.

Electrochemical impedance spectroscopy (EIS) measurements were utilized to investigate the mechanism of photocurrent improvement. The semicircle diameter generally indicates the carrier transfer resistance. In Figure 6, all Nyquist plots of the composites presented as semicircle, the corresponding arc radius of EIS Nyquist plots all decreased compared to that of bare anatase TiO_2, which is consistent with the photocurrent output. Among all photocatalysts, sample T1-NGQDs exhibited the smallest semicircle while sample T0 the largest. This result is demonstrative of more effective carrier separation and transfer process in the heterojunctions [47,48]. Thus, it could be concluded that the percentage of exposed {001} facet indeed had different effects on the electronic properties of the composites, which might be attributed to the different interfacial interaction between NGQDs and TiO_2 with different facet compositions.

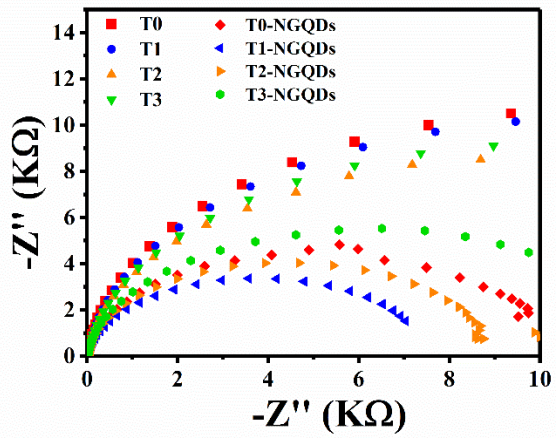

Figure 6. Electrochemical impedance spectroscopy (EIS) Nyquist plots of different TiO_2 samples without and with NGQDs decoration.

Photoluminescence (PL) emission spectrum could help to directly understand the carrier behaviors and observe the radiative recombination of charge carriers [49,50]. Generally, PL emission signals are caused by the photo-induced carrier recombination process. Lower intensity is relevant to better photocatalytic performance. All peaks shape similarly in Figure 7. After decorating NGQDs, the composites exhibited a slight decrease in the PL intensity, compared to the bare anatase, which was probably due to the efficient electron transfer from the CB band of anatase to NGQDs. Thus, the trapping and recombination of charge carriers could be hindered.

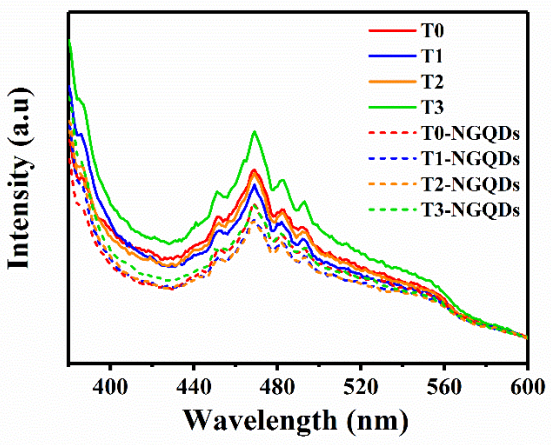

Figure 7. PL spectra of different TiO_2 samples without and with NGQDs decoration.

2.4. Photocatalytic Performance

The photocatalytic performances of all samples were evaluated for RhB photodegradation under visible light irradiation after achieving absorption-desorption balance in the dark, as seen from Figure 8. Obviously, the photocatalytic degradation efficiency of the TiO_2/NGQDs heterojunctions was greatly enhanced compared with that of the bare anatase TiO_2. Among the composites, approximately 96% of the dye was photo-degraded by the T1-NGQDs within 3 h. The degradation process followed the pseudo-first-order kinetics:

$$-\ln\left(\frac{c}{c_0}\right) = \mathrm{kt} \quad (1)$$

where k is equal to the corresponding slope of the fitting line, representing the rate constant indicative of the photocatalytic efficiency. To prove the efficiency of sample T1-NGQDs, the photocatalytic degradation activity of other three organic pollutants including methylene blue (MB), methyl orange (MO), and phenol (Phe) were compared. It demonstrated that the T1-NGQDs exhibited high photocatalytic activity for degrading MB dye as well as other common organic species (including phenol, colorless aqueous solution), shown in Figure S6.

The calculated k values of different samples are shown in Figure 8c (the red column corresponds to the bare anatase TiO_2 and the blue column to the composites). Before decorating NGQDs, sample T2 and T3 exhibited nearly the same constant rate, higher than that of T0 and T1. RhB could be easily absorbed on the titania surface with reactive {001} facet exposure, leading to subsequent dye self-photosentization process decomposing RhB under visible light irradiation [51–53].

After decoration of NGQDs, it was found that the values were much higher, and the calculated k of T1-NGQDs reached the highest, about 0.8 h^{-1}. The multiple times of the k values of the anatase TiO_2 with and without NGQDs decoration were then calculated, shown in Figure 8d. Notably, it was shown that the times decreased with the increase of the exposed {001} facet percentage in TiO_2, which is consistent with the photocurrent variation in Figure 5c. The same law illustrates the photocatalytic degradation performance depends greatly on the interfacial charge carrier separation and transfer rate, demonstrative of the significant donor-acceptor interaction between NGQDs and {101} facets. At the same time, it was supposed that the different roles of {001} and {101} facets in separating the

photogenerated electron-hole are unignorable, since the hybrid containing TiO_2 with 56% {001} facets exhibited a higher reaction rate value than that with 12% {001} facets.

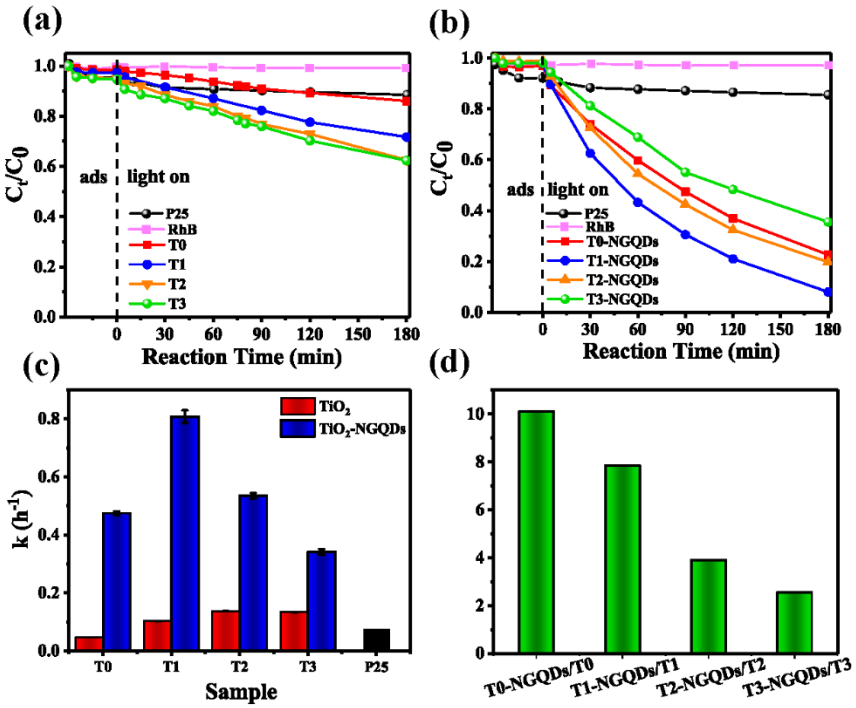

Figure 8. The photocatalytic degradation of RhB for different samples under visible light irradiation. Change of the relative concentration (C_t/C_0) of RhB in (**a**) bare anatase TiO_2, (**b**) TiO_2/NGQDs composites as a function of irradiation time up to 180 min. (**c**) Plot of k ($\ln(C_0/C_t)$) values for RhB degradation in different samples. (**d**) The times of the k values of the anatase with and without NGQDs decoration.

2.5. Photocatalytic Mechanism

The schematic representation of the electron-hole separation and transfer in TiO_2/NGQDs heterojunction composites during the photocatalytic reaction is shown in Scheme 1. Under visible light irradiation, both NGQDs and anatase TiO_2 of avoidable intrinsic defects were capable to generate photo-excited electrons. Obviously, the narrow energy gaps for NGQDs allow for rich hot electrons to produce when the excitation wavelength is larger than 420 nm. According to the measured band potential values, the energy levels in Figure 4d further demonstrate that the band configuration contributes to electron injections from the CB level of TiO_2 to the LUMO of NGQDs. The donor-acceptor interaction was greatly promoted due to the full contact and C–O–Ti formation between NGQDs and TiO_2. The appropriate band alignments explain for the reason why the photocatalytic activities were all enhanced after depositing NGQDs on the surface of TiO_2, compared to that of bare TiO_2.

On the other hand, for bare TiO_2, it was found that the anatase TiO_2 with the higher percentage of exposed {001} facet owned a much better photocatalytic performance which is due to the high activity of the {001} facet. However, the reaction rate value (k) achieved the highest for T1-NGQDs rather than T3-NGQDs. The different variation trend of k value in bare TiO_2 and TiO_2/NGQDs heterojunctions imply the possible influence of facets in the interfacial electron transfer process. It revealed that the photo-excited electron and holes behave differently in TiO_2, where electrons could be easily trapped in the {101} facet while holes tend to run to the {001} facet. Since NGQDs are a good electron transport medium, its deposition on the titania surface with more percentages of exposed {101} facets could result in a higher electron transfer efficiency, which is consistent with the increasing multiple times of photocurrent and also k values with and without NGQDs decoration. Simultaneously, the different roles of {101} and {001} facets in anatase TiO_2 on charge carrier separation is not negligible, considering that the k value of T1-NGQDs is higher than that of T0-NGQDs. By comparing the degradation activity

of TiO_2 before and after NGQDs decoration, it could be concluded that there is a synergistic effect of facet-manipulated electron-hole separation in TiO_2 and donor-acceptor interaction in GQDs/TiO_2 on the visible light driven photocatalytic performance.

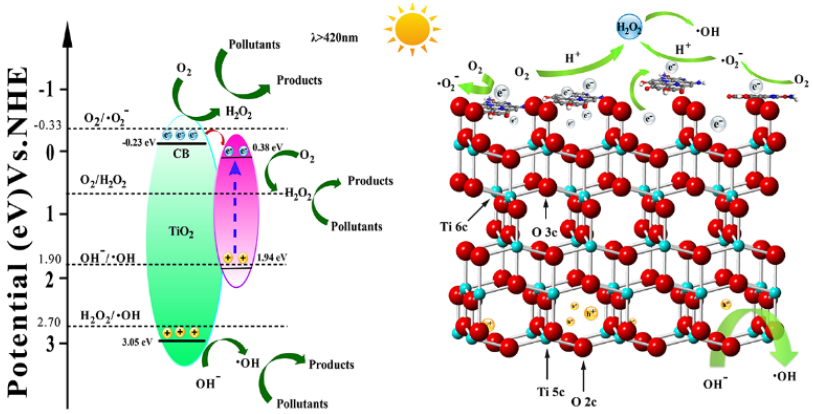

Scheme 1. Schematic illustration of the proposed band alignment and interfacial electron transfer process for the TiO_2/NGQDs heterojunction composites under visible light irradiation (λ > 420 nm).

3. Materials and Methods

3.1. Synthesis of Anatase TiO_2

The anatase TiO_2 with different exposed percentages of {001} and {101} facets were prepared via the traditional hydrothermal method. Typically, different volumes (0.2, 0.4, and 0.8 mL) of hydrofluoric acid (≥40.0%. Sinopharm Chemical Reagent Co.,Ltd, Shanghai, China) were added into the mixture of tetrabutyl titanate (5 mL; ≥99.0%, Aladdin, Shanghai, China) and ethanol (8 mL). After stirring for 30 min, the mixture was then transferred into a 50 mL Teflon-lined autoclave and heated at 180 °C for 24 h. After that, the products were collected by centrifugation, followed by being rinsed several times with absolute ethyl alcohol and dried at 60 °C overnight. The obtained anatase TiO_2 co-exposed with {001} and {101} facets were named as T1, T2, and T3 respectively. To prepare TiO_2 with the {101} dominating plane, the same procedure was conducted but with 0.4 mL of H_2O, which was named T0.

3.2. Synthesis of NGQDs

The NGQDs were prepared according to a one-step hydrothermal process reported by Sun and co-workers [54]. In a typical run, 1.44 g of urea (AR, Aladdin, Shanghai, China) and 1.68 g of citric acid (GR, Aladdin, Shanghai, China) were dissolved in 40 mL of deionized water (DI water). The solution was transferred into a 50 mL Teflon-lined stainless autoclave and heated at 180 °C for 8 h. The final product was centrifuged several times at 10,000 rpm for 5 min with absolute alcohol. The obtained NGQDs precipitate was dried at 80 °C for 1 h to obtain the NGQDs powders.

3.3. Synthesis of TiO_2/NGQDs Heterojunction Composites

An ultrasonic-hydrothermal method was used to prepare the TiO_2/NGQDs heterojunction photocatalysts. A certain amount of TiO_2 and GQDs at a low doping level (1.0 wt%) was added into 40 mL of DI water. The suspension solution was placed in an ultrasonic bath for 30 min and then transferred into a 50 mL Teflon-lined stainless autoclave by heating at 120 °C for another 2 h. After centrifuging several times with DI water and being dried at 60 °C overnight, the final powders were named as T0-NGQDs, T1-NGQDs, T2-NGQDs, and T3-NGQDs, respectively.

3.4. Characterization

The XRD patterns of all samples were recorded with a PAN analytical X'Pert Pro MPD diffractometer (Pananalytical, Holland) using Cu-Kα radiation (λ = 0.1541 nm), and the data was collected from 20° to 80° (2θ). UV-vis diffuse reflectance spectroscopy (DRS) were taken at room temperature measured using $BaSO_4$ as the reference on a UV-3150 spectrophotometer (Shimadzu, Kyoto, Japan). The photoluminescence (PL) spectroscopy was performed using a RF-5301pc fluorescence spectroscopy (Shimadzu, Kyoto, Japan). Band gap energies were calculated by analysis of the Tauc-plots resulting from Kubelka–Munk transformation of absorption spectra. High resolution transmission electron microscope (HRTEM) were conducted by a Phillips/FEI Tecnai F20 S-TWIN TEM (Hillsborough, OR, USA) instrument operating at 200 kv. X-ray photoelectron spectroscopy (XPS) measurements were carried out on an ESCALAB 250 Xi (Thermo Scientific, MA, USA) using non-monochromatized Mg-Kα X-ray as the excitation source. The binding energies for the samples were calibrated by setting the measured binding energy of C 1s to 284.60 eV. The Raman spectra were measured on a LabRAM HR Evolution (Horiba, Tokyo, Japan) at room temperature using the 532 nm line of an argon ion laser as the excitation source.

3.5. Photocatalytic Performance

The photocatalytic performance of the as-synthesized photocatalysts were examined under a 300 W Xe lamp (PLS-SXE 300/300 UV, Perfect Light, Shanghai, China) equipped with a 420 nm cut-off filter as the visible light irradiation source. A total of 15 mg of catalysts were added into 50 mL of a 10.0 $mg{\cdot}L^{-1}$ solution of different dyes: Rhodamin B (RhB), methylene blue (MB), methyl orange (MO), and phenol (Phe) (Sinopharm Chemical Reagent Co. Ltd., Shanghai, China). The molar concentration was 0.026, 0.031, 0.030, and 0.11 mmol/L, respectively. Before irradiation, the suspension was stirred in the dark to ensure the adsorption-desorption equilibrium of RhB on the surface of the photocatalyst.

3.6. Photoelectrochemical Measurements

The photocurrent measurements, electrochemical impedance spectroscopy (EIS) and Mott–Schottky experiments were conducted on an electrochemical analyzer (CHI 660C work station, CHI, Shanghai, China). The employed standard three-electrode configuration included a platinum plate (as the counter electrode), an Ag/AgCl electrode (as the reference electrode), and a working electrode. The working electrodes were prepared as follows: 40 mg of powders and 5 mg of $Mg(NO_3)_2{\cdot}6H_2O$ (≥98%; Alfa Aesar, Shanghai, China) were dispersed in 100 mL of isopropanol. The suspension was ultrasound for 1 h. A clean SnO_2 transparent conductive glass doped with fluorine, FTO (as cathode) facing the stainless-steel anode was then immersed into this suspension. The distance between the two electrodes was fixed at about 5 cm. The Mg^{2+} adsorbed samples suspension was loaded in a quartz vessel as the electrolyte, and the electrophoresis process was performed at 60 V for 120 s. After the electrophoretic deposition (EPD) process, the prepared electrodes were washed by ethanol and deionized water several times and dried at room temperature. A 350 W xenon lamp with a cut-off filter (λ > 420 nm) was used as a light source and placed 20 cm away from the working electrode. The working electrode was immersed in 0.1 M Na_2SO_4 aqueous solution. The EIS measurements were performed over a range from 0.01 to 1000 Hz at 0.2 V, and the amplitude of the applied potential in each case was 5 mV.

4. Conclusions

In summary, nitrogen-doped graphene quantum dots were successfully deposited onto the surface of anatase TiO_2 with different percentages of exposed {001} facets to form TiO_2/GQDs heterojunction composites. The photocatalytic performances of the hybrid containing TiO_2 with 56% {001} facets exhibited the highest reaction rate value under visible light irradiation. The successful decoration of NGQDs on the TiO_2 surface extended the light absorption edge into the visible light region. Due

to Ti–O–C formation and high electron conductivity of NGQDs, the photocurrent responses of the composites were all enhanced obviously, compared to that of the bare samples. Meanwhile, the different roles of {101} and {001} facets in anatase TiO_2 on charge carrier separation was also not negligible. The improved photocatalytic activity was due to the synergistic effect of facet-manipulated electron-hole separation in TiO_2 and the remarkable donor-acceptor interaction between NGQDs and the electron-rich {101} facet. The existence of the {101} facet contributed to the interfacial electron transfer that played a vital role in improving the photocatalytic activity of the NGQDs/TiO_2 heterojunctions. Furthermore, the existence of both facets in anatase assisted the further enhancement of photocatalytic performance. This work provided a new clue to improve the interfacial charge transfer in faceted semiconductor related heterojunctions.

Supplementary Materials: The following are available online at http://www.mdpi.com/2073-4344/9/4/345/s1, Figure S1: (a) Slab model of anatase TiO_2 single crystal. (b) Equilibrium model of anatase TiO_2 single crystal. (Calculation method of the percentage of {001} facets). Figure S2: (a) Raman spectra of different TiO_2 samples without and with NGQDs decoration. (b) Raman spectra of T1 before and after decoration of NGQDs. The inset in Figure S2 b is the enlargement of 1200–1700 cm^{-1} of T1-NGQDs. Figure S3: TEM images of (a) T0, (b) T1, (c) T2, and (d) T3. Figure S4: (a) TEM image, (b) HRTEM image, (c) AFM image, (d) UV-vis spectra and PL spectra of the GQDs (the excitation wavelength is 365 nm), (e) Raman spectra, and (f) XRD pattern of NGQDs. The inset in (a) is the size distribution of NGQDs. The inset in (b) is the autocorrelated HRTEM lattice images recorded. Figure S5: HRTEM images of the anatase TiO_2 decorate with NGQDs. Figure S6: (a) The photocatalytic degradation of different pollutants for T1-NGQDs, (b) plot of k values for different pollutants degradation in T1-NGQDs.

Author Contributions: The manuscript was written through contributions of all authors. N.-Q.O., H.-J.L. designed the experiments; N.-Q.O., B.-W.L., B.-J.G. and X.S. performed the experiments and analyzed the data; N.-Q.O. and H.-J.L. wrote the paper; D.-J.Q. revised the paper. X.W., Y.J. and J.Y. acted as supervisor.

Funding: This research was funded by National Natural Science Foundation of China (51572173, 51602197, 51771121 and 51702212), Shanghai Municipal Science and Technology Commission (16060502300, 16JC1402200 and 18511110600), Shanghai Academic/Technology Research Leader Program (19XD1422900), Shanghai Eastern Scholar Program (QD2016014).

Conflicts of Interest: The authors declare no conflicts of interest.

References

1. Tang, H.; Prasad, K.; Sanjinès, R.; Schmid, P.E.; Lévy, F. Electrical and optical properties of TiO_2 anatase thin films. *J. Appl. Phys.* **1994**, *75*, 2042–2047. [CrossRef]
2. Xu, M.; Gao, Y.; Moreno, E.M.; Kunst, M.; Muhler, M.; Wang, Y.; Idriss, H.; Woll, C. Photocatalytic activity of bulk TiO_2 anatase and rutile single crystals using infrared absorption spectroscopy. *Phys. Rev. Lett.* **2011**, *106*, 138302. [CrossRef] [PubMed]
3. Yu, J.; Low, J.; Xiao, W.; Zhou, P.; Jaroniec, M. Enhanced Photocatalytic CO_2-Reduction Activity of Anatase TiO_2 by Co-exposed {001} and {101} Facets. *J. Am. Chem. Soc.* **2014**, *136*, 8839–8842. [CrossRef]
4. Tachikawa, T.; Yamashita, S.; Majima, T. Evidence for crystal-face-dependent TiO_2 photocatalysis from single-molecule imaging and kinetic analysis. *J. Am. Chem. Soc.* **2011**, *133*, 7197–7204. [CrossRef] [PubMed]
5. Selcuk, S.; Selloni, A. Facet-dependent trapping and dynamics of excess electrons at anatase TiO_2 surfaces and aqueous interfaces. *Nat. Mater.* **2016**, *15*, 1107–1118. [CrossRef]
6. Chen, Q.; Ma, W.; Chen, C.; Ji, H.; Zhao, J. Anatase TiO_2 mesocrystals enclosed by (001) and (101) facets: Synergistic effects between Ti^{3+} and facets for their photocatalytic performance. *Chem. Eur. J.* **2012**, *18*, 12584–12589. [CrossRef]
7. Hyam, R.S.; Lee, J.; Cho, E.; Khim, J.; Lee, H. Effect of Annealing Environments on Self-Organized TiO_2 Nanotubes for Efficient Photocatalytic Applications. *Nanosci. Nanotechnol.* **2012**, *12*, 8908–8912. [CrossRef]
8. Wang, X.; Sun, G.; Li, N.; Chen, P. Quantum dots derived from two-dimensional materials and their applications for catalysis and energy. *Chem. Soc. Rev.* **2016**, *45*, 2239–2262. [CrossRef]
9. Wegner, K.D.; Hildebrandt, N. Quantum dots: Bright and versatile in vitro and in vivo fluorescence imaging biosensors. *Chem. Soc. Rev.* **2015**, *44*, 4792–4834. [CrossRef]
10. Yuan, F.; Li, S.; Fan, Z.; Meng, X.; Fan, L.; Yang, S. Shining carbon dots: Synthesis and biomedical and optoelectronic applications. *Nano Today* **2016**, *11*, 565–586. [CrossRef]

11. Crake, A.; Christoforidis, K.C.; Godin, R.; Moss, B.; Kafizas, A.; Zafeiratos, S.; Durrant, J.R.; Petit, C. Titanium dioxide/carbon nitride nanosheet nanocomposites for gas phase CO_2 photoreduction under UV-visible irradiation. *Appl. Catal. B* **2019**, *242*, 369–378. [CrossRef]
12. Olowoyo, J.O.; Kumar, M.; Jain, S.L.; Babalola, J.O.; Vorontsov, A.V.; Kumar, U. Insights into Reinforced Photocatalytic Activity of the CNT–TiO_2 Nanocomposite for CO_2 Reduction and Water Splitting. *J. Phys. Chem. C* **2018**, *123*, 367–378. [CrossRef]
13. Rimoldi, L.; Giordana, A.; Cerrato, G.; Falletta, E.; Meroni, D. Insights on the photocatalytic degradation processes supported by TiO_2/WO_3 systems. The case of ethanol and tetracycline. *Catal. Today* **2019**, *328*, 210–215. [CrossRef]
14. Zheng, X.T.; Ananthanarayanan, A.; Luo, K.Q.; Chen, P. Glowing graphene quantum dots and carbon dots: Properties, syntheses, and biological applications. *Small* **2015**, *11*, 1620–1655. [CrossRef]
15. Freeman, R.; Finder, T.; Bahshi, L.; Gill, R.; Willner, I. Functionalized CdSe/ZnS QDs for the detection of nitroaromatic or RDX explosives. *Adv. Mater.* **2012**, *24*, 6416–6421. [CrossRef]
16. Long, R.; Casanova, D.; Fang, W.-H.; Prezhdo, O.V. Donor-Acceptor Interaction Determines the Mechanism of Photo-Induced Electron Injection from Graphene Quantum Dots into TiO_2: Stacking Supersedes Covalent Bonding. *J. Am. Chem. Soc.* **2017**, *139*, 2619–2629. [CrossRef]
17. Wang, W.-S.; Wang, D.-H.; Qu, W.-G.; Lu, L.-Q.; Xu, A.-W. Large Ultrathin Anatase TiO_2 Nanosheets with Exposed {001} Facets on Graphene for Enhanced Visible Light Photocatalytic Activity. *J. Phys. Chem. C* **2012**, *116*, 19893–19901. [CrossRef]
18. Wang, F.; Wu, Y.; Wang, Y.; Li, J.; Jin, X.; Zhang, Q.; Li, R.; Yan, S.; Liu, H.; Feng, Y.; et al. Construction of novel Z-scheme nitrogen-doped carbon dots/{0 0 1} TiO_2 nanosheet photocatalysts for broad-spectrum-driven diclofenac degradation: Mechanism insight, products and effects of natural water matrices. *Chem. Eng. J.* **2019**, *356*, 857–868. [CrossRef]
19. Wang, W.; Ni, Y.; Xu, Z. One-step uniformly hybrid carbon quantum dots with high-reactive TiO_2 for photocatalytic application. *J. Alloys Compd.* **2015**, *622*, 303–308. [CrossRef]
20. Baker, D.R.; Kamat, P.V. Photosensitization of TiO_2 Nanostructures with CdS Quantum Dots: Particulate versus Tubular Support Architectures. *Adv. Funct. Mater.* **2009**, *19*, 805–811. [CrossRef]
21. Kenrick, J.; Williams, C.A.N.; Yan, X.; Li, L.-S.; Zhu, X. Hot Electron Injection from Graphene Quantum Dots to TiO_2. *ACS Nano* **2013**, *7*, 1388–1394.
22. Yang, N.; Liu, Y.; Wen, H.; Tang, Z.; Zhao, H.; Li, Y.; Wang, D. Photocatalytic Properties of Graphdiyne and Graphene Modified TiO_2: From Theory to Experiment. *ACS Nano* **2013**, *7*, 1504–1512. [CrossRef]
23. Pan, D.; Jiao, J.; Li, Z.; Guo, Y.; Feng, C.; Liu, Y.; Wang, L.; Wu, M. Efficient Separation of Electron–Hole Pairs in Graphene Quantum Dots by TiO_2 Heterojunctions for Dye Degradation. *ACS Sustain. Chem. Eng.* **2015**, *3*, 2405–2413. [CrossRef]
24. Ma, Y.; Chen, A.Y.; Xie, X.; Wang, X.; Wang, D.; Wang, P.; Li, H.-J.; Yang, J.; Li, Y. Doping effect and fluorescence quenching mechanism of N-doped graphene quantum dots in the detection of dopamine. *Talanta* **2018**, *196*, 563–571. [CrossRef] [PubMed]
25. Yu, S.; Zhong, Y.Q.; Yu, B.Q.; Cai, S.Y.; Wu, L.Z.; Zhou, Y. Graphene quantum dots to enhance the photocatalytic hydrogen evolution efficiency of anatase TiO_2 with exposed {001} facet. *Phys. Chem. Chem. Phys.* **2016**, *18*, 20338–20381. [CrossRef]
26. Zheng, L.; Su, H.; Zhang, J.; Walekar, L.S.; Vafaei Molamahmood, H.; Zhou, B.; Long, M.; Hu, Y.H. Highly selective photocatalytic production of H_2O_2 on sulfur and nitrogen co-doped graphene quantum dots tuned TiO_2. *Appl. Catal. B* **2018**, *239*, 475–484. [CrossRef]
27. Jiang, B.; Tian, C.; Zhou, W.; Wang, J.; Xie, Y.; Pan, Q.; Ren, Z.; Dong, Y.; Fu, D.; Han, J.; et al. In situ growth of TiO_2 in interlayers of expanded graphite for the fabrication of TiO_2-graphene with enhanced photocatalytic activity. *Chem. Eur. J.* **2011**, *17*, 8379–8387. [CrossRef]
28. Liu, L.; Jiang, Y.; Zhao, H.; Chen, J.; Cheng, J.; Yang, K.; Li, Y. Engineering Coexposed {001} and {101} Facets in Oxygen-Deficient TiO_2 Nanocrystals for Enhanced CO_2 Photoreduction under Visible Light. *ACS Catal.* **2016**, *6*, 1097–1108. [CrossRef]
29. Tian, F.; Zhang, Y.; Zhang, J.; Pan, C. Raman Spectroscopy: A New Approach to Measure the Percentage of Anatase TiO_2 Exposed (001) Facets. *J. Phys. Chem. C* **2012**, *116*, 7515–7519. [CrossRef]

30. Li, H.-J.; Sun, X.; Xue, F.; Ou, N.; Sun, B.-W.; Qian, D.-J.; Chen, M.; Wang, D.; Yang, J.; Wang, X. Redox Induced Fluorescence On–Off Switching Based on Nitrogen Enriched Graphene Quantum Dots for Formaldehyde Detection and Bioimaging. *ACS Sustain. Chem. Eng.* **2018**, *6*, 1708–1716. [CrossRef]
31. Qu, A.; Xie, H.; Xu, X.; Zhang, Y.; Wen, S.; Cui, Y. High quantum yield graphene quantum dots decorated TiO_2 nanotubes for enhancing photocatalytic activity. *Appl. Surf. Sci.* **2016**, *375*, 230–241. [CrossRef]
32. Rajender, G.; Kumar, J.; Giri, P.K. Interfacial charge transfer in oxygen deficient TiO_2-graphene quantum dot hybrid and its influence on the enhanced visible light photocatalysis. *Appl. Catal. B* **2018**, *224*, 960–972. [CrossRef]
33. Shen, K.; Xue, X.; Wang, X.; Hu, X.; Tian, H.; Zheng, W. One-step synthesis of band-tunable N, S co-doped commercial TiO_2/graphene quantum dots composites with enhanced photocatalytic activity. *RSC Adv.* **2017**, *7*, 23319–23327. [CrossRef]
34. Wang, W.; Xu, D.; Cheng, B.; Yu, J.; Jiang, C. Hybrid carbon@TiO_2 hollow spheres with enhanced photocatalytic CO_2 reduction activity. *J. Mater. Chem. A* **2017**, *5*, 5020–5029. [CrossRef]
35. Xu, C.; Han, Q.; Zhao, Y.; Wang, L.; Li, Y.; Qu, L. Sulfur-doped graphitic carbon nitride decorated with graphene quantum dots for an efficient metal-free electrocatalyst. *J. Mater. Chem. A* **2015**, *3*, 1841–1846. [CrossRef]
36. Han, S.; Hu, X.; Wang, J.; Fang, X.; Zhu, Y. Novel Route to Fe-Based Cathode as an Efficient Bifunctional Catalysts for Rechargeable Zn-Air Battery. *Adv. Energy Mater.* **2018**, *8*, 1800955. [CrossRef]
37. Li, H.-J.; Ou, N.-Q.; Sun, X.; Sun, B.-W.; Qian, D.-J.; Chen, M.; Wang, X.; Yang, J. Exploitation of the synergistic effect between surface and bulk defects in ultra-small N-doped titanium suboxides for enhancing photocatalytic hydrogen evolution. *Catal. Sci. Technol.* **2018**, *8*, 5515–5525. [CrossRef]
38. Rimoldi, L.; Pargoletti, E.; Meroni, D.; Falletta, E.; Cerrato, G.; Turco, F.; Cappelletti, G. Concurrent role of metal (Sn, Zn) and N species in enhancing the photocatalytic activity of TiO_2 under solar light. *Catal. Today* **2018**, *313*, 40–46. [CrossRef]
39. Ding, H.; Yu, S.B.; Wei, J.S.; Xiong, H.M. Full-Color Light-Emitting Carbon Dots with a Surface-State-Controlled Luminescence Mechanism. *ACS Nano* **2016**, *10*, 484–491. [CrossRef]
40. Ding, H.; Wei, J.S.; Zhang, P.; Zhou, Z.Y.; Gao, Q.Y.; Xiong, H.M. Solvent-Controlled Synthesis of Highly Luminescent Carbon Dots with a Wide Color Gamut and Narrowed Emission Peak Widths. *Small* **2018**, *14*, e1800612. [CrossRef]
41. Yang, H.; Wang, P.; Wang, D.; Zhu, Y.; Xie, K.; Zhao, X.; Yang, J.; Wang, X. New Understanding on Photocatalytic Mechanism of Nitrogen-Doped Graphene Quantum Dots-Decorated $BiVO_4$ Nanojunction Photocatalysts. *ACS Omega* **2017**, *2*, 3766–3773. [CrossRef]
42. Deming, C.P.; Mercado, R.; Gadiraju, V.; Sweeney, S.W.; Khan, M.; Chen, S. Graphene Quantum Dots-Supported Palladium Nanoparticles for Efficient Electrocatalytic Reduction of Oxygen in Alkaline Media. *ACS Sustain. Chem. Eng.* **2015**, *3*, 3315–3323. [CrossRef]
43. Safardoust-Hojaghan, H.; Salavati-Niasari, M. Degradation of methylene blue as a pollutant with N-doped graphene quantum dot/titanium dioxide nanocomposite. *J. Clean. Prod.* **2017**, *148*, 31–36. [CrossRef]
44. Wang, S.; Cole, I.S.; Li, Q. Quantum-confined bandgap narrowing of TiO_2 nanoparticles by graphene quantum dots for visible-light-driven applications. *Chem. Commun.* **2016**, *52*, 9208–9211. [CrossRef]
45. Wang, D.; Chen, J.-F.; Dai, L. Recent Advances in Graphene Quantum Dots for Fluorescence Bioimaging from Cells through Tissues to Animals. *Part. Part. Syst. Charact.* **2015**, *32*, 515–523. [CrossRef]
46. Zou, X.; Liu, M.; Wu, J.; Ajayan, P.M.; Li, J.; Liu, B.; Yakobson, B.I. How Nitrogen-Doped Graphene Quantum Dots Catalyze Electroreduction of CO_2 to Hydrocarbons and Oxygenates. *ACS Catal.* **2017**, *7*, 6245–6250. [CrossRef]
47. Li, H.-J.; Qian, D.J.; Chen, M. Templateless Infrared Heating Process for Fabricating Carbon Nitride Nanorods with Efficient Photocatalytic H2 Evolution. *ACS Appl. Mater. Interfaces* **2015**, *7*, 25162–25170. [CrossRef]
48. Yan, M.; Zhu, F.; Gu, W.; Sun, L.; Shi, W.; Hua, Y. Construction of nitrogen-doped graphene quantum dots-$BiVO_4$/g-C_3N_4Z-scheme photocatalyst and enhanced photocatalytic degradation of antibiotics under visible light. *RSC Adv.* **2016**, *6*, 61162–61174. [CrossRef]
49. Liu, J.; Li, J.; Sedhain, A.; Lin, J.; Jiang, H. Structure and Photoluminescence Study of TiO_2 Nanoneedle Texture along Vertically Aligned Carbon Nanofiber Arrays. *J. Phys. Chem. C* **2008**, *112*, 17127–17132. [CrossRef]
50. Nadica, D.; Abazovic, M.I.C.O.; Dramicanin, M.D. Photoluminescence of Anatase and Rutile TiO_2 Particles. *J. Phys. Chem. B* **2006**, *110*, 25366–25370.

51. Hu, C.; Zhang, X.; Li, X.; Yan, Y.; Xi, G.; Yang, H.; Bai, H. Au photosensitized TiO_2 ultrathin nanosheets with {001} exposed facets. *Chem. Eur. J.* **2014**, *20*, 13557–13560. [CrossRef]
52. Li, K.; Xu, Y.; He, Y.; Yang, C.; Wang, Y.; Jia, J. Photocatalytic fuel cell (PFC) and dye self-photosensitization photocatalytic fuel cell (DSPFC) with BiOCl/Ti photoanode under UV and visible light irradiation. *Environ. Sci. Technol.* **2013**, *47*, 3490–3497. [CrossRef]
53. Wang, X.; Xia, R.; Muhire, E.; Jiang, S.; Huo, X.; Gao, M. Highly enhanced photocatalytic performance of TiO_2 nanosheets through constructing TiO_2/TiO_2 quantum dots homojunction. *Appl. Surf. Sci.* **2018**, *459*, 9–15. [CrossRef]
54. Qu, D.; Zheng, M.; Du, P.; Zhou, Y.; Zhang, L.; Li, D.; Tan, H.; Zhao, Z.; Xie, Z.; Sun, Z. Highly luminescent S, N co-doped graphene quantum dots with broad visible absorption bands for visible light photocatalysts. *Nanoscale* **2013**, *5*, 12272–12278. [CrossRef]